Kainic Acid Pig Model of Hippocampal Epilepsy

Filip Mivalt[1*×], Daniela Maltais[1*], Inyong Kim[1], Jiwon Kim[1], Patrik Began[1], Andrea Duque Lopez[1], Veronika Krakorova[1], Bailey Winter[1], Cheng Yen Kuo[1], Shelja Sharma [1], Elizabeth S. Harty[1], Luke H. Kim[1], Nicholas Gregg[1], Dan Montonye[2], Christopher Gow[2], Kai Miller[3], Jamie Van Gompel[3], Kent Leyde[4], Vaclav Kremen[1,5], Su-youne Chang[1,2†], Gregory A. Worrell[1†×]

[1]Department of Neurology, BNEL (Bioelectronics Neurophysiology & Engineering Lab), Mayo Clinic, Rochester, MN, USA
[2]Department of Comparative Medicine, Mayo Clinic, Rochester, MN, USA
[3]Department of Neurologic Surgery, Mayo Clinic, Rochester, MN, USA
[4]Cadence Neuroscience Inc. Seattle, WA, USA
[5]Czech Institute of Informatics, Robotics, and Cybernetics, Czech Technical University in Prague, Prague, Czech Republic

* Authors contributed equally
† Senior authors: Su-youne Chang and Gregory A. Worrell
× Corresponding authors:
- Filip Mivalt (mivalt.filip@mayo.edu)
- Gregory A. Worrell (worrell.gregory@mayo.edu)

Key words: epilepsy, pig, kainic acid, implantable neurostimulators

Abstract

Translational animal models that can accommodate human-scale implantable devices are essential for advancing chronic brain stimulation and sensing applications. This study establishes a kainic acid (KA)-induced porcine model of mesial temporal lobe epilepsy (mTLE) using a neurotechnology platform integrating clinical imaging, stereotactic surgery, and a fully implantable device for chronic monitoring.

In six KA-treated and one saline-control pig bilateral hippocampus (HPC) and anterior thalamus (ANT) local field potentials were monitored using an implantable device, along with synchronized video recordings. Histology was performed to assess neuronal injury and hippocampal reorganization.

Intra-hippocampal KA infusion induced acute status epilepticus (6/6 pigs). Surviving KA-treated pigs (4/6) were monitored for a total of 386 days with spontaneous seizures occurring in three subjects. A total of 2,733 hippocampal seizures were recorded with a seizure duration of 27.16±17.62 seconds. All subjects exhibited bilateral interictal epileptiform discharges, predominantly in the lesioned hemisphere ($p < 0.0001$). Histological analysis revealed cytoarchitectural disorganization consistent with hippocampal injury.

This porcine model recapitulates many of the electrophysiological and structural hallmarks of human mTLE. The platform provides a powerful translational bridge for developing novel sensing and stimulating neuromodulation strategies in freely behaving large animals using human-scale implantable devices.

Glossary of Abbreviations

Abbreviation	Definition
ANT	Anterior Nucleus of Thalamus
AUC	Area Under the Curve
CT	Computed Tomography
CV	Cresyl Violet
DBS	Deep Brain Stimulation
DG	Dentate Gyrus
FBTCS	Focal to Bilateral Tonic-Clonic Seizures
FGATIR	Fast Gray Matter Acquisition T1 Inversion Recovery
HPC	Hippocampus
ICC	Intraclass Correlation Coefficient
IEDs	Interictal Epileptiform Discharges
INSR	Implantable Neural Sensing and Recording
KA	Kainic Acid
LFP	Local Field Potential
MPRAGE	Magnetization-Prepared Rapid Gradient Echo
MRI	Magnetic Resonance Imaging
mTLE	mesial Temporal Lobe Epilepsy
MTT	Mammillothalamic Tract
PPV	Positive Predictive Value
SE	Status Epilepticus
SPEP	Single Pulse Evoked Potentials

Introduction

Epilepsy is a prevalent neurological disorder affecting approximately 50 -60 million people worldwide [1].-Beyond recurrent seizures, epilepsy is often associated with psychiatric comorbidities including anxiety, depression [2]–[4], memory impairments [3], cognitive deficits [2], [3], and sleep disturbances [5]–[7], reflecting complex network pathophysiology [2]. These comorbidities are thought to arise from circuit reorganization [8], neuroinflammation [9], neurodegeneration [10], [11], and functional abnormalities [12]. Mesial temporal lobe epilepsy (mTLE) exemplifies the challenges of drug-resistant epilepsy and is a compelling target for advanced neuromodulation [13]–[22].

Electrical brain stimulation is an established therapy for drug-resistant epilepsy reducing seizure burden with the anterior nucleus of the thalamus (ANT) and hippocampus (HPC) being common neuromodulation targets. However, complete seizure freedom is rare and stimulation parameter optimization is a lengthy process taking months to years [18], [19], [21]. The extended optimization timeline is impacted by the sporadic occurrence of seizures as the main outcome measure, and the inaccuracy of patient seizure self-reports [18], [19], [21]–[23]. These challenges motivate the development of the next-generation devices [13], [16].

Developing and testing next-generation neuromodulation devices for epilepsy can be accelerated with an appropriate animal model that can accommodate human-sized devices, replicate human physiology, behavior, and therapeutic responses (predictive validity). Rodent models have been extensively used in epilepsy research [24]. However, rodents are not a suitable translational model for human device testing, due to their small size and limited neuroanatomical complexity. Large animals, such as dogs [25], [26] and pigs [27]–[29] provide a gyrencephalic brain structure and sufficient size to support multimodal imaging, surgical procedures, and implantable devices designed for humans.

Chemical induction of seizures with intrahippocampal infusion of kainic acid (KA) has been widely applied in rodent models [24], [30] and recently demonstrated in a porcine model [28]. Localized intra-amygdala or intra-hippocampal KA infusion induces pathological features of human hippocampal sclerosis including neuronal cell loss, gliosis, granule cell dispersion, and aberrant mossy fiber sprouting [31], [32].

Here we describe a KA-porcine model of hippocampal epilepsy and a neurotechnology platform integrating advanced neuroimaging protocols, image-guided stereotactic targeting, fully implantable four-lead neural sensing, stimulating and recording (INSR) device for synchronized video and local field potential (LFP) recordings in behaving large animals (Figure 1.).

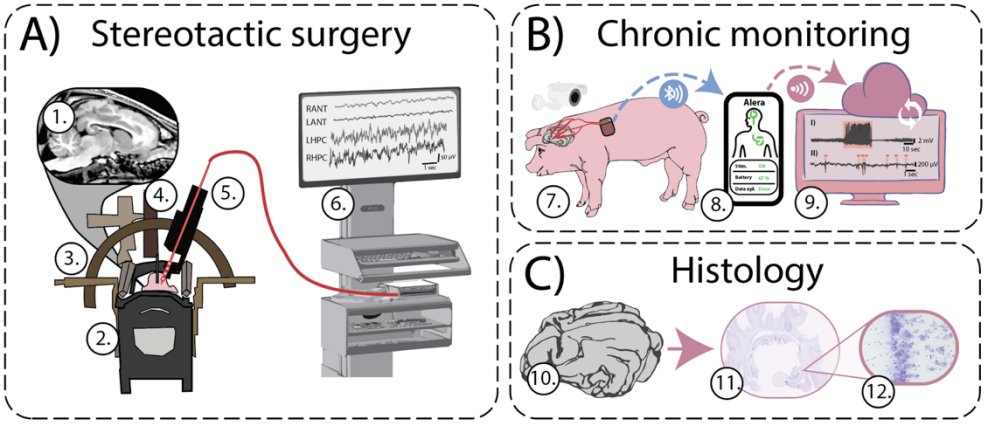

Figure 1: Neurotechnology Platform for Development of Chronic Large Animal Epilepsy Models. A) Stereotactic implantation surgery using 1) 3 Tesla pre-op MRI imaging, 2) a custom MRI compatible stereotactic frame for head fixation, 3) stereotactic Leksell frame compatible with Brainlab stereotactic planning software (Brainlab AG, Munich, Germany) for electrode targeting, 4) Microinjector for kainic acid infusion and 5) Electrode and cannula delivery system to implant lead electrodes into bilateral ANT and HPC and inject KA into HPC. 6) intra-operative workstation for electrophysiology monitoring, perform single pulse electrical stimulation, and tracking the local field potential (LFP) changes induced by KA infusion. **B) Chronic electrophysiology monitoring** 7) implanted animals were chronically monitored with synchronized video and LFP recordings using. an implantable four lead neural stimulating and recording device that wirelessly transfers LFP recordings using a Low Energy Bluetooth to 8) Android phone application and 9) cloud with automated LFP signal processing for seizure and IED detection. **C) Brain Histology** was performed to investigate structural changes in the 10) explanted brains for 11) gross structural and 12) microscopic histologic changes.

Results

We developed a porcine mTLE model using stereotactic intrahippocampal KA injection. The pre-operative imaging, stereotactic targeting, intra-op recording, and chronic recordings in freely behaving animals were demonstrated with systems designed for human epilepsy.

Subjects

Seven domestic Yorkshire pigs (Sus scrofa), 6 intact females (S1-6) and one neutered male (S7) with a mean weight 18.80 ± 5.34 kg received an intrahippocampal KA injection. One control pig (S7) received a saline injection. Animals were chronically monitored using synchronized video and a four lead implantable neural stimulating recording (INSR) device designed for humans.

The animal research took place at Mayo Clinic, Rochester, MN, USA. All study procedures adhered to the National Institutes of Health Guidelines for Animal Research (Guide for the Care and Use of Laboratory Animals) and were approved by the Institutional Animal Care and Use Committee under (IACUC) under IACUC protocol A00006870.

Acute Surgery and KA Induction of Status Epilepticus

Four leads were implanted in bilateral HPC and ANT using Magnetic Resonance Imaging (MRI) guided stereotactic surgery.

The acute LFPs demonstrated lower amplitudes and power spectral density in the ANT compared to the HPC (ANT: 0.80 ± 3.92 μV/Hz vs HPC: 8.77 ± 5.83 μV/Hz; $p < 10^{-6}$, Mann-Whitney U-test) consistent with reports from human recordings [14].

A single pulse evoked potential (SPEP) protocol was used in two pigs (S5-S6) to intraoperatively to evaluate ANT-HPC connectivity [33], [34]. The ANT-HPC connectivity demonstrated functional circuit asymmetry in latencies and amplitudes (ANT → HPC latency vs HPC → ANT latency: 16.64 ± 5.88 ms vs. 8.44 ± 2.25 ms, $p < 0.0001$, Mann-Whitney U-test). Interestingly, HPC → HPC SPEP demonstrated higher magnitude compared to the ANT →HPC (1.81 ± 0.23 μV vs 2.41±0.25 μV, U = 965.0, $p < 0.0001$, Mann-Whitney U-test) (Figure 2).

Intrahippocampal KA infusion (1μg/μl) into the HPC (S1: 16 μl, S2,3,5,6: 6 μl, S4: 4 μl) elicited onset of electrographic IEDs and seizures. The initial focal electrographic seizure was localized to the injection site before the seizure propagated to the ANT and contralateral HPC (Figure 2). Seizures and prolonged SE were acutely observed in all animals except the saline control (S7).

The targeting accuracy was confirmed with post-operative Computed Tomography imaging and histology

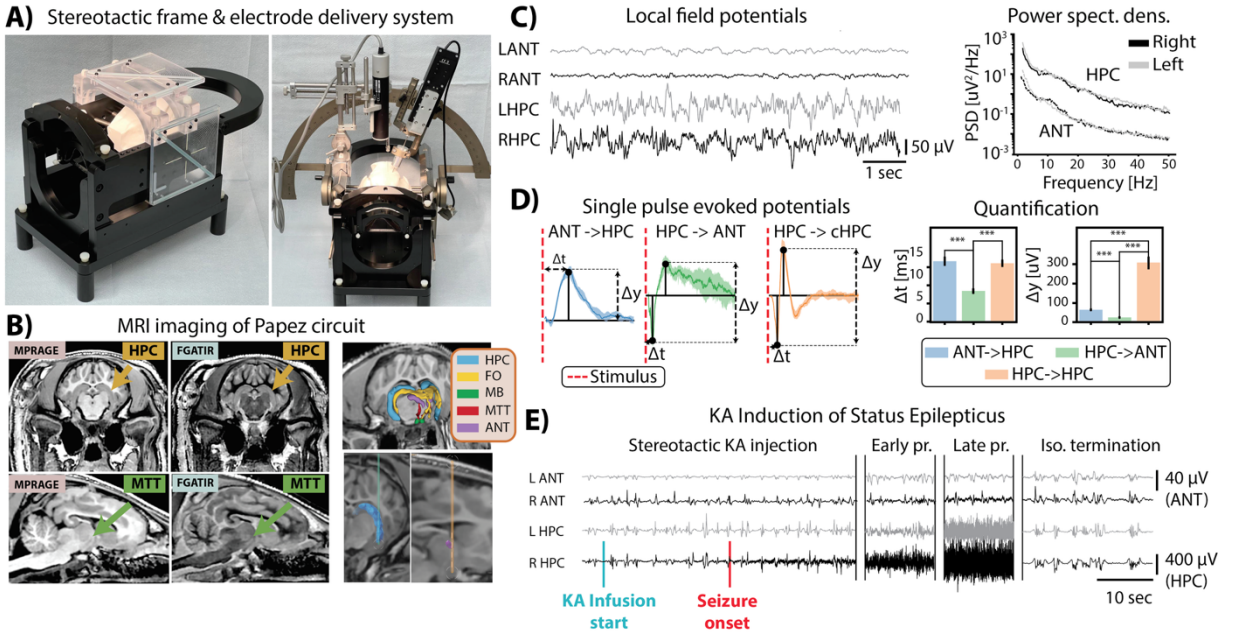

Figure 2 Intraoperative Electrophysiology of Papez Circuit and Acute Status Epilepticus A) MRI compatible stereotactic frame. A custom MRI compatible machined plastic head frame with jaw and skull set screws for head fixation with N-bar fiducial box and compatible with Brainlab stereotactic software, Leksell arc-frame and, manipulator, micro-injection delivery and manual or computer-controlled electrode drive (w/o canula) for electrode lead delivery. **B) MRI scans utilized for pre-operative planning.** MPRAGE and FGATIR were utilized for targeting and volumetric rendering of HPC, fornix (FO), mamillary bodies (MB), MTT and ANT. **C) Representative intra-operative local field potential** traces from bilateral anterior nucleus of the thalamus (ANT) and hippocampus (HPC) with corresponding power spectral density. The ANT LFPs are lower amplitude with decreased broadband power compared to HPC. **D)** Single Pulse Evoked Potentials from ANT to HPC (ANT→HPC), HPC to ANT (HPC→ANT) and HPC to contralateral HPC (HPC→cHPC). The latency of initial negative response first peak (Δt) and peak to peak magnitude(Δy) were evaluated. **E) KA Induction of Status Epilepticus.** Injection of KA provoked prolonged status epilepticus that was terminated

with 3.5% Isoflurane after 20 minutes. The onset of right (R) HPC seizure after KA infusion. The seizure propagates into the left (L) HPC and R ANT.

Recovery and Acute Seizure Dynamics

In KA-pigs during the first hour upon emergence from anesthesia, bilateral hippocampal seizure activity persisted and occasionally progressed to focal to bilateral tonic-clonic seizures (FBTCS). These seizures included tonic extension of a forelimb, lateral head deviation, and generalized clonic movements. Limb movements resembling "running" were also intermittently observed. While these overt behavioral manifestations were primarily confined to the first hour, electrographic seizure activity in the HPC persisted for up to 12 hours post-operatively.

Subjects S1 and S6 were euthanized within 12 hours of surgery. Subject S1 received 16 µl KA injection followed by refractory SE that was unresponsive to intravenous diazepam. Continued electrographic seizures were recorded post-operatively by the INSR device and the animal was euthanized. Subject S6 (6µl) had prolonged post-operative seizures and received diazepam (0.5 - 1 mg/kg). The pig experienced cardiopulmonary arrest, and resuscitation was unsuccessful. Autopsy revealed cardiac pathology, including dilated ventricles with thin walls, possibly contributing to cardiopulmonary arrest and death.

The control animal (S7) did not develop acute seizure or status epilepticus.

Automated Epileptiform Seizure and IED Detection

Automated IED and seizure detectors developed for humans and canines were validated in pigs against manual annotations by a human expert (Figure 3A). The automated IED detection algorithm achieved a sensitivity of 0.87 and a Positive Predictive Value (PPV) of 0.68 when compared to the expert annotations. The automated seizure detector achieved a Receiver Operating Characteristic Area Under the Curve (AUC) of 0.93 and a Precision-Recall Curve AUC of 0.84 when compared to the expert annotations (Figure 3A).

Chronic Monitoring, Seizures and IEDs in behaving pig mTLE model

The four KA-treated surviving pigs (S2-5) and the control pig (S7) were maintained and monitored using video and the INSR device recordings for a total of 433 days (S2: 271 days, S3: 10 days, S4: 19 days, S5: 86 days, S7 (control): 47 days) (Table 1.).

Interictal epileptiform discharges (IEDs) were observed in all surviving subjects. The IED morphologies included spike and wave discharges, high frequency ripple oscillations [35] and polyspikes—all of which have been reported in previous KA seizure models [28], [36], [37] (Figure 3). We observed independent and synchronous spontaneous IEDs with higher hourly IED rate in the lesioned HPC (lesioned 352.68 ± 338.49 vs. contralateral 174.59 ± 269.71, $p < 0.0001$, Mann-Whitney U-test) in all subjects including the control.

Three out of four of the KA-treated pigs had spontaneous seizures (S2, S3, S5) occurring an average of 10.33 ± 3.40 days post-KA infusion. A total of 2,733 (683.25 ± 694.82)

electrographic seizures were recorded (Table 1). The average electrographic seizure frequency was 32.37 ± 43.67 seizures per day, and average duration was 27.16 ± 17.62 seconds. (Table 1). We observed multiple behavioral seizure correlates including brief behavioral arrest, generalized tonic-clonic convulsive seizures and myoclonic jerks.

The control animal (S7) did not exhibit spontaneous electrographic seizures during the 47-day chronic monitoring period. However, chronic monitoring did show spontaneous IEDs, indicating that the mechanical insult of the fluid injection alone is sufficient to create a focus of network hyperexcitability.

S3 and S4 were euthanized on day 10 and 19 after the implant surgery due to wound infections around the INSR device.

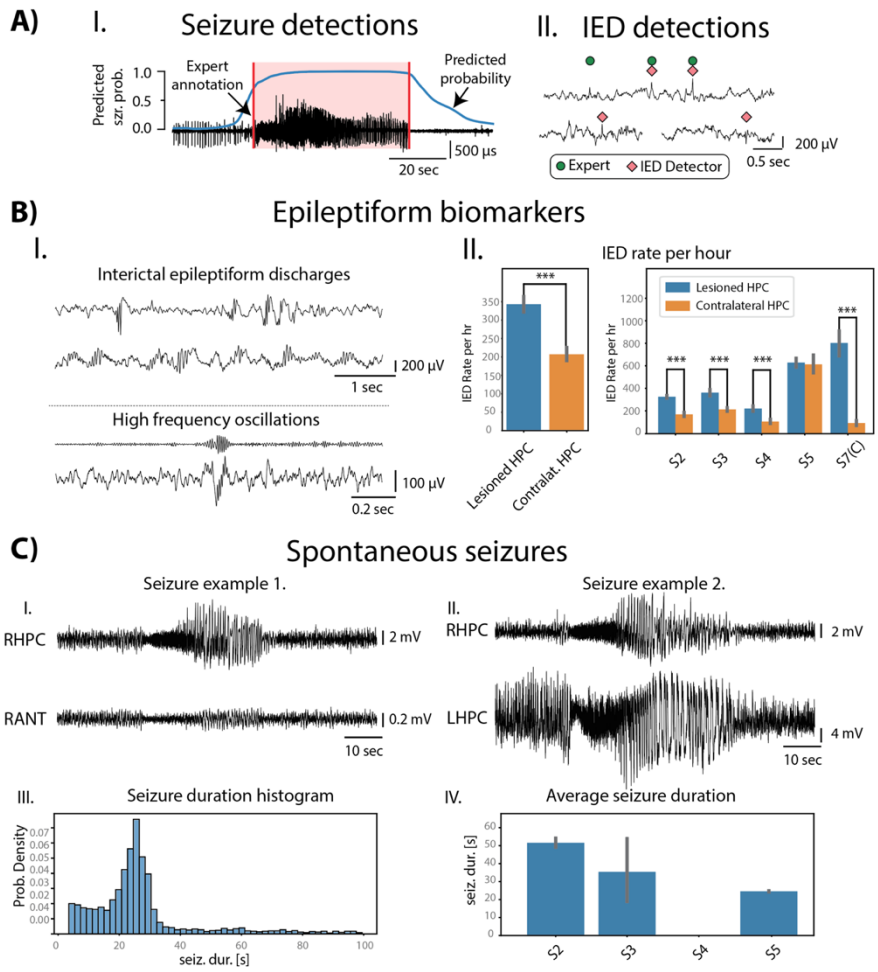

Figure 3. Spontaneous Interictal Epileptiform Discharges (IED) and Seizures in Chronic Pig Model. A) Examples of automated seizure and IED detectors compared to human expert annotations. I. A representative seizure detection, showing the algorithm's predicted probability (blue line) overlaid on the local field potential (LFP) signal and the expert's manual annotation (red shaded area). **II.** A representative IED detection, with automated detections (red diamonds) and expert annotations (green circles) marked on the LFP trace. **B) Spontaneous IEDs** during chronic monitoring with implanted device. ***I.*** Representative example of IEDs, and high frequency ripple oscillations (filtered between 80 Hz – 270 Hz). ***II.*** IED rates in the left and right HPC, with higher hourly IED rate in the right HPC (KA & control injection site) compared to the contralateral HPC. **C) Spontaneous Seizures** during chronic monitoring. ***I.*** A representative right hippocampus (RHPC) seizure with recording from RHPC and right anterior nucleus of thalamus (RANT). ***II.*** RHPC seizure with propagation to LHPC. ***III.*** A histogram of automatically detected seizure durations. *IV.* A bar plot showing average seizure duration for each subject. Note, S4 and the control S7 did not have any seizure detections.

Table 1: Seven domestic Yorkshire pigs, six females (F) and one male (M) were used for intrahippocampal Kainic Acid (KA; 1 µg/µl) model. S7 was a control pig. The weight at the time of implant; total injected KA dose; hippocampal Interictal epileptiform discharges (IEDs), seizures, and status epilepticus (SE) (* - p<0.05; ** - p<0.01, *** p<0.001, Mann-Whitney – lesioned HPC vs Contralateral HPC).

Sub.	Weight [kg]	Volume [µl]	Sex	Maintained [days]	Spontaneous IEDs per Hour		Spontaneous Electrographic Seizures			Events
					Lesioned HPC	Contralat. HPC	Total Seizures	Seizure duration [s]	Onset [days]	
S1	9.4	16	F	0	n/a	n/a	-	n/a	n/a	Euthanized with uncontrolled SE
S2	14.0	6	F	271	**339.90±173.02 *****	130.24 ± 201.87	1,101	33.51 ± 27.73	9 days	SE, IED, SZ
S3	19.0	6	F	10	**361.35±98.09 *****	212.77 ± 56.04	24	23.80 ± 25.07	7 days	SE, IED, SZ
S4	21.0	4	F	19	**218.52±259.21 ****	104.20 ± 201.59	0	-	-	SE, IED
S5	19.0	6	F	86	607.39±590.62	622.43 ± 295.11	1,608	24.04 ± 9.08	15 days	SE, IED, SZ
S6	21.8	6	F	0	n/a	n/a	0	-	-	SE, IED, SZ Cardiopulmonary Arrest
S7	27.4	0	M	47	**794.20±246.46 *****	94.90±48.48	-	-	-	IED

Histology

The histology of the KA-treated HPC revealed significant pathological changes in the hippocampal subfields (CA1,CA3, and dentate gyrus DG) including pyramidal and granular cell loss, dispersion, and the presence of pyknotic nuclei [38] (Figure 4). Additionally, pyramidal cell dispersion and pyknotic cells wereobserved in the contralateral CA1. The pathologic changes for each structure specifically included:

- CA1: extensive pyramidal cell dispersion, non-specific patches of pyramidal cell loss and presence of dark pyknotic nuclei
- CA3: disorganization, dispersion and non-specific patches of pyramidal cell loss
- DG: granular cell dispersion, cell loss, pyknotic nuclei

Despite the visually observed qualitative changes, a linear mixed-effects model accounting for variability between slices and reviewers found no significant difference in neuron counts between KA-treated HPC and contralateral HPC (Estimate = -2.08, SE = 38.46, p = 0.95). The average-measure of visual review concordance using intraclass correlation coefficient (ICC), ICC(C,3)) was 0.616, 95% CI [0.244, 0.820], F(23, 46) = 2.60, p = 0.0028 indicating moderate reliability across raters

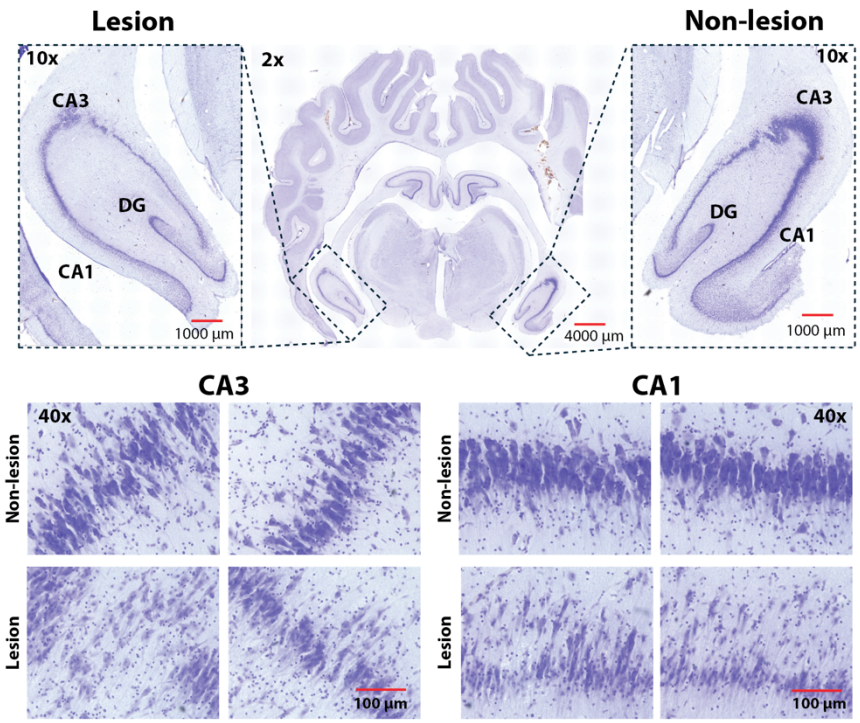

Figure 4. Histology samples of the lesioned vs control HPC. Coronal brain sections from four Yorkshire pig (Sus Scrofa) were processed by cresyl violet staining. Representative images at low (2x) magnification of the lesioned and contralateral (non-lesioned) hemispheres are shown. Boxed areas highlight the CA3, DG, and CA1 regions of the hippocampus at a higher (10x) magnification. Below (40x): Pyramidal cell disorganization and dispersion were predominant in the CA3 and CA1 lesioned region, compared to their contralateral control. Non-specific patches of pyramidal cell loss were observed in the pyramidal cell layer of the CA3 and in the CA1 region. Hippocampal regions are labeled for reference. CA1: Cornu Ammonis 1; DG: Dentate Gyrus; CA3: Cornu Ammonis 3; Hi: Hilus. Scale bars: 4000 µm at 2x, 1000 µm at 10x, 100 µm at 40x.

Discussion

In this study, we developed a porcine KA model of mTLE and demonstrated chronic electrophysiological and video monitoring. The model demonstrated key pathological and electrophysiological features of human mTLE, making it a promising platform for translational research and development of next-generation neuromodulation devices. Large animal models of epilepsy represent a vital step in the development and testing of implantable technologies designed for human use.

Our study builds upon the prior work of Zhu et al. [28], who established the feasibility of the porcine intra-hippocampal KA model with intermittent electrophysiological recordings under light anesthesia. The primary novelty of our work is the development of an integrated platform for clinical-grade imaging and acute intra-operative and chronic electrophysiology. Key distinctions include the implementation of a chronic, fully implantable, human-grade INSR device, the specific targeting and functional characterization of the Papez circuit (ANT-HPC, HPC-HPC) using SPEPs, and continuous 24/7 synchronized video-LFP monitoring in freely behaving animals. The substantially higher electrographic seizure burden captured in our cohort (2,733 seizures in 3 animals) compared to the prior study (46 seizures in 4 animals) [28] is likely attributable to our continuous monitoring methodology, which captures events that would be missed by intermittent 2-hour daily recordings under anesthesia.

KA Dose and Seizure Outcomes We investigated a range of intra-hippocampal KA doses (4µl, 6µl, and 16µl) to establish a porcine mTLE model. All doses successfully induced acute status epilepticus (SE); however, the 16µl dose resulted in refractory SE that required euthanasia, indicating this dose was suprathreshold. The 6µl dose, used in most pigs (4/6), successfully induced chronic, spontaneous seizures in surviving animals, demonstrating its effectiveness in producing the desired mTLE phenotype. While this dose group did experience mortality, the causes were attributed to non-dose-related factors, including post-operative infection and pre-existing cardiac pathology. Therefore, while our findings show that a 6µl dose is effective, future studies with a larger cohort are required to fully optimize the protocol for consistent long-term outcomes. Notably, the emergence of IEDs following a saline-only infusion suggests that the injection procedure itself acts as a potentially epileptogenic insult, independent of KA neurotoxicity. A 6 µl saline injection is not a benign event; it is a volumetric and traumatic injury that causes acute tissue displacement, blood-brain barrier disruption, and a subsequent cascade of neuroinflammation and reactive gliosis.

Seizure and IED Detector Validation The IED and seizure detection algorithms were previously validated in both human and canines [13], [39]. Here the detectors yielded good performance in the pig model without further hyperparameter tuning. We acknowledge the sample size is a limitation and a potential area for more extensive validation in future work.

Behavioral Seizure Correlates Our characterization of behavioral seizures focused primarily on overt events with clear motor manifestations, such as focal to bilateral tonic-clonic seizures that included jerking and falling, or sudden awakenings from sleep. A detailed classification of seizures impacting awareness was beyond the scope of this initial study. Therefore, a systematic assessment for seizures with more subtle behavioral correlates, such as those limited to impaired awareness, was not performed. However, we did note subtle behavioral changes, such as a sudden cessation of activity, which post-hoc inspection of the LFP confirmed were correlated with hippocampal electrographic seizures. Developing and implementing specific behavioral assays to formally assess awareness-impairing seizures is a key objective for future studies.

Comparison with Human mTLE A further limitation is the nature of the latent period in this model. While a latent period was observed, with spontaneous seizures beginning an average of 10.33 days post-insult, this is shorter than the months or years often seen in human acquired epilepsy [8], [32]. This accelerated timeline is likely a feature of the direct intra-hippocampal KA infusion, which serves as a potent and targeted insult, potentially speeding up the network reorganization that leads to chronic epilepsy [30]. Future studies could explore lower KA doses to investigate if a more prolonged latent period can be established, which may more closely model the human condition.

Implications for Neuromodulation Device Development The porcine mTLE model provides a unique opportunity to advance neuromodulation therapies. The relatively large brain size and ability to accommodate electrode leads and INSR devices designed for humans will be useful for testing neuromodulation and sensing paradigms [13], [14], [17], [23], [40]–[44] .

Limitations and Future Directions This study is limited by the small sample size, which may affect the generalizability of findings. We were unable to assess post-KA SPEP changes intra-

operatively due to persistent focal status epilepticus masking any evoked activity. This leaves a gap in understanding the effect of KA on evoked responses. Despite qualitative evidence of cell loss and disorganization in the lesioned hippocampus, quantitative analysis did not confirm a significant difference between the hemispheres. This discrepancy may reflect methodological limitations or the propagation of seizure activity causing secondary pathological changes in the contralateral control side.

Future studies should include a larger cohort to validate findings and further refine KA dosing for improved survival and chronic seizure outcomes. Lastly, incorporating behavioral assessments, such as responsiveness, memory, mood, and sleep alongside electrophysiological monitoring could enhance our understanding of seizure-related comorbidities in this model [45], [46]. Finally, exploring additional neuromodulation targets within the Papez circuit could provide insights into broader therapeutic applications for epilepsy-related cognitive and emotional deficits.

Conclusion

We successfully demonstrated a pig model of mTLE and chronic electrophysiology with synchronized video monitoring of epileptiform activity. This model demonstrates reliable induction of chronic epilepsy through targeted hippocampal KA injections, with spontaneous IEDs and seizures observed in surviving animals. The model supports chronic monitoring in freely behaving animals and in the future can be used for testing novel sensing and stimulation paradigms. Our findings underscore the translational potential of a porcine mTLE model for addressing unmet clinical needs of novel stimulation therapies in drug-resistant epilepsy.

Methods

Animals

Animals were housed on a 12/12 light cycle with ad libitum access to water and once-daily feeding. Animals were housed in temperature-controlled rooms (45% humidity, 21°C temperature) with elevated floors that met all size, material and sanitation requirements according to Guide for the Care and Use of Laboratory Animals [47]. Animals were provided mats and daily enrichment via assorted treats, chew toys, and human interaction. Animals were socially housed, except during post-surgery period. Animals were assessed daily by a team of veterinarians and technicians. All animals were humanely euthanized at the conclusion of the study.©∫

Pre- and Post-Surgical Imaging

Pre-operative planning was conducted using a 3.0 Tesla MRI (GE Medical Systems). Magnetization-prepared rapid gradient echo (MPRAGE) and fast gray matter acquisition T1 inversion recovery (FGATIR) sequences were selected for their enhanced gray-white matter contrast [48], [49]. These MRI sequences, commonly used for electrode lead placement planning

in human deep brain stimulation (DBS), provided visualization of the mammillothalamic tract (MTT) for precise direct ANT targeting [50]. Post-operative electrode placement was confirmed through computed tomography (CT) (Somatom Flash, Siemens Inc.), co-registered with the pre-operative MRI. Images were analyzed in Brainlab (Brainlab AG, Munich, Germany) and 3D Slicer [51] (Figure 2).

Stereotactic & Recording Instrumentation

A custom stereotactic surgery platform consisting of an MRI compatible, machined plastic head fixation frame (Supplement) and a modified Leksell arc-frame (Elekta Inc., Stockholm, Sweden) compatible with a stereotactic targeting software Brainlab (Brainlab AG, Munich, Germany) was used for electrode implantation and KA infusion. The stereotactic frame was designed to accommodate up to 40 kg pigs, with 15 kg – 25 kg being an optimal weight.

A 16-channel Cadence Navia Workstation (Cadence Neuroscience Inc., Seattle, WA) LFP sensing (0.1 Hz - 1 kHz bandpass, 8 kHz sampling rate, 24-bit resolution,) and programmable stimulation was used for acute intraoperative electrophysiology monitoring.

Chronic LFP monitoring was conducted using a fully implantable, 16-channel Cadence Alera INSR device (Cadence Neuroscience Inc., Seattle, WA). This system records from two digitally selected bipolar derivations (0.1 Hz - 1 kHz bandpass, 8 kHz sampling rate, 16-bit resolution and a 2 Gbit nonvolatile memory). The INSR system includes the implantable device, a handheld programmer/controller for wireless bi-directional data transfer via Bluetooth Low Energy, and a charger (Figure 5).

Stereotactic Surgery and Kainic Acid Infusion

Pre-operative MRI scans and stereotactic targeting software (Brainlab AG, Munich, Germany) and porcine brain atlas [52] were used for segmentation and targeting of HPC and ANT, both common targets in mTLE neuromodulation therapy [13], [16], [18], [19], [21], [22]. Four 4-electrode leads were implanted through skull burr holes, secured with "dog-bone" anchors and bone screws. Anesthesia was induced and maintained with isoflurane for the stereotactic surgery. The initial four pigs (S1-S4) underwent KA infusion under continuous low-level isoflurane and the last two pigs (S5, S6) with a combined ketamine-xylazine anesthesia protocol following a 30-minute isoflurane washout (Table 1). This anesthesia change was implemented because of concern that isoflurane, a GABA-A agonist and direct kainate receptor antagonist, anti-convulsant properties could pharmacologically confound the acute KA status epilepticus [30], [53].

One pig (S7) underwent an identical stereotactic surgery and intra-hippocampal infusion with an equivalent volume (6 µl) of sterile saline instead of KA as a control for the effects of the hippocampal injection procedure itself.

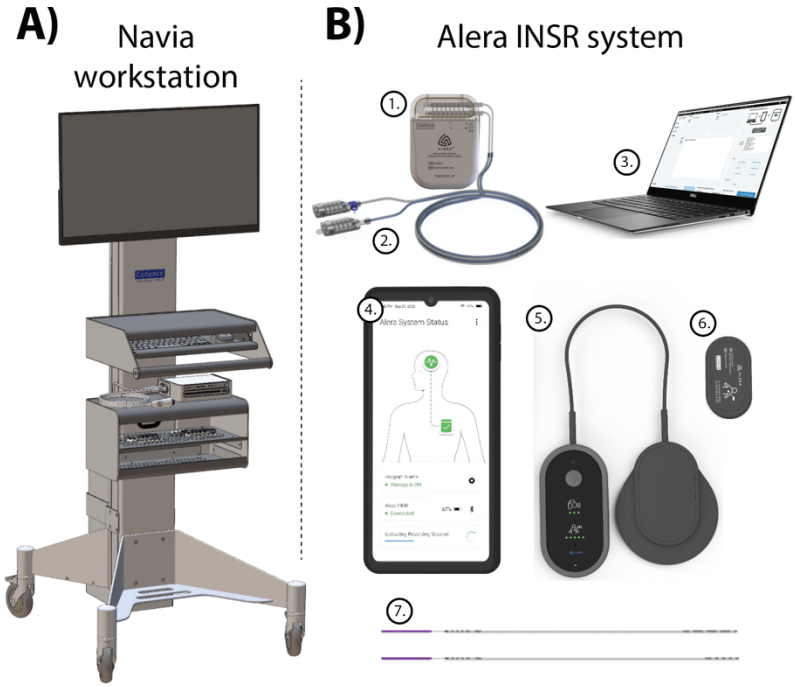

C) Technical specifications

Sensing	Navia Workstation	Alera INSR
Sampling rate	8 kHz	8 kHz, 2 kHz, 500 Hz
Number of channels	16	16 (4 x 4 contacts)
Recording modes	continuous	continuous, scanning
Input range	±0.7 V	±30 mV
Bandpass	0.1 Hz - 1 kHz	0.1 Hz - 1 kHz
Resolution	24 bit (100 nV)	16-bit (1.8 µV)
Memory	-	2 Gbit (nonvolatile)
Stimulation		
Type	constant current	constant current
Waveform	biphasic, charge-balanced	biphasic, charge-balanced
Compliance voltage	±15 V	±12 V
Stimulation frequency	0.1 Hz to 166 Hz	0.1 Hz to 166 Hz
Pulse width	62.5 µs to 500 µs	62.5 µs to 500 µs
Resolution	0.1 mA to 20 mA	0.1 mA to 20 mA
Max number of interleaved waveforms	8	8
Electrodes	**3.5 mm**	**7 mm**
Diameter	1.35 mm	1.35 mm
Tip length	2 mm	2 mm
Contact length	2 mm	2 mm
Contact spacing	1.5 mm	5 mm

Figure 5: Local Field Potential (LFP) Recording Instrumentation. A) Navia Workstation (NW) is a 16-channel LFP recording, and stimulation platform. The NW enables high fidelity LFP sensing and recording (0.1 – 1000 Hz: Sampling 8 kHz) and programmable electrical stimulation. **B) Alera Implantable Neural Stimulation and Recording (INSR) system**. The INSR is a rechargeable, 16-channel sensing (0.1 – 1000 Hz: Sampling up to 8 kHz, 2 Gb memory), stimulation and recording device. The Alera system includes: 1) 16 channel INSR supporting four leads (4-contacts each) with 2) electrode extensions with skull mounted bifurcation port, 3) programmer (Tablet computer), 4) controller (Android mobile phone), 5) charger, 6) control magnet and 7) electrode leads with 3.5 mm and 7 mm span. The INSR can wirelessly communicate with the controller, relaying information such as the INSR battery level, operational status, and recording status; additionally, the controller may store recorded data downloaded from the INSR. The programmer is used to generate stimulation therapy programs that are uploaded to the INSR via the controller. **C) Detailed device specifications**.

At surgery the externalized electrode leads were connected to the bedside electrophysiology workstation for acute monitoring using sterile electrode extensions. KA in six pigs and sterile saline in the control pig were stereotactically delivered to the hippocampus along a separate track using a Hamilton syringe positioned 1-2 mm from the HPC recording electrode contact. KA (1µg/µl) or saline was administered in 2 µL increments at a rate of 1 µl per minute, with a 10-minute interval between doses. We investigated 16 µl, 6 µl, and 4 µl KA total dose and 6 µl saline dose in the control pig. Focal hippocampal status was terminated with intravenous benzodiazepines (0.5 – 1.0 mg/kg) and isoflurane anesthesia after 20 minutes.

After conclusion of the acute recording, the four electrode leads were tunneled under the skin and connected to bifurcation ports mounted on the skull and two-wire extensions (8-contact extensions) were tunneled to the implantable neural sensing and recording (INSR) device (Cadence Neuroscience Inc., Seattle, WA) positioned behind the right scapula. Post-surgical CT scans were used to confirm electrode placement.

LFP Recording and Analysis

Cadence Navia workstation was utilized to record LFPs and probe the Papez circuit using single pulse evoked potentials (SPEP). The LFP referential recordings from the ANT and HPC using the 16 electrode contacts (4 contacts on each of the 4 implanted leads) were obtained during surgery at baseline and during intrahippocampal KA infusion. The SPEP were measured as a response to a single pulse stimulation with 6 mA current, 250µs pulse width at 0.1 Hz. A visual review was utilized to intra-operatively identify seizures.

INSR devices were implanted behind the right scapula and used for chronic LFP recording with a range of sampling rates (500 Hz, 2 kHz or 8 kHz). The sampling rate of 500 Hz was utilized for chronic LFP recordings. Higher sampling rates were utilized to record short LFP recordings of 1 minute to 10 minutes periodically. The INSR enables stimulation from the 16 contacts and LFP recording from two digitally selected bipolar electrode derivations (Figure 5).

Bipolar LFP channel recordings were derived from the raw acute LFP traces recorded using the Navia workstation for each brain location. The workstation LFPs were subsequently filtered using anti-aliasing filter and downsampled to 500 Hz for further analysis. A narrow-band notch filter with quality factor 10 was utilized to suppress 60 Hz powerline noise in the workstation LFP data. Downsampled workstation LFP data and longitudinal INSR LFP data were stored at 500 Hz sampling, and the same signal processing protocol was utilized for both workstation and INSR data.

LFP signals were filtered between 2 Hz and 100 Hz using a 101st-order finite response (FIR) filter. Previously developed Python libraries [13], [14], [45] were utilized to process LFP signals. An IED and seizure detector previously validated in humans and canines [13], [39] was validated for the pig. A human expert annotated IEDs and seizures from long-term recordings (222 IEDs and 42 seizures) for validation. All data annotated were utilized solely for testing of the previously developed detectors. In this study no additional training or tuning of detector hyperparameters was performed. After validation in the pig the IED and seizure detection algorithms were utilized to detect seizures and IEDs in the freely behaving pigs.

Histology

The explanted brains were fixed in 4% paraformaldehyde and stored in 30% sucrose in 1X Phosphate-Buffered Saline. Brains were frozen with dry ice and cut to 60-µm thick coronal sections on a sliding microtome (Leica Biosystems, Wetzlar, Germany) in serial order starting from the corpus callosum anteriorly to the caudal end of the ventral hippocampus. Brain sections were immersed in a 1% cresyl violet (CV) acetate solution (Sigma-Aldrich, C5042) for approximately 5 minutes. Subsequently, the slides were immersed in 70% EtOH for 10 minutes. Further removal of excess stain was achieved by immersing the sections in 95% EtOH with 150 ul of acetic acid for approximately 3 minutes, followed by two series of 5-minute baths of 100% EtOH and xylene. Finally, the slices were cover slipped using Eukitt® Quick-hardening mounting medium (03989, Sigma-Aldrich), and imaged under a microscope (Keyence, BZ-X800). The protocol was inspired by [54]–[56]. Slides were visually and quantitatively examined

for differences between the control and the KA-treated CA1, CA3 and dentate gyrus regions using available pig brain atlases. [52], [57].

To assess the effect of KA on neuronal counts in hippocampal subregions (CA1, CA3, and DG), three blinded reviewers manually quantified cells using ImageJ [58]. A hippocampal subsection was selected within a defined hippocampal subregion in the KA-lesioned hippocampal and the corresponding region in the contralateral hippocampus were identified with equidistant positions along the anterior-posterior axis. The interrater reliability amongst three reviewers was assessed using the intraclass correlation coefficient (ICC), based on a two-way random-effects model with a consistency definition.

References

[1] World Health Organization, *Epilepsy: a public health imperative*. World Health Organization, 2019.

[2] B. P. Hermann, A. F. Struck, K. Dabbs, M. Seidenberg, and J. E. Jones, "Behavioral phenotypes of temporal lobe epilepsy," *Epilepsia Open*, vol. 6, no. 2, pp. 369–380, June 2021.

[3] B. Bell, J. J. Lin, M. Seidenberg, and B. Hermann, "The neurobiology of cognitive disorders in temporal lobe epilepsy," *Nat. Rev. Neurol.*, vol. 7, no. 3, pp. 154–164, Mar. 2011.

[4] J. F. Tellez-Zenteno, S. B. Patten, N. Jetté, J. Williams, and S. Wiebe, "Psychiatric comorbidity in epilepsy: a population-based analysis," *Epilepsia*, vol. 48, no. 12, pp. 2336–2344, Dec. 2007.

[5] C. W. Bazil, B. Legros, and E. Kenny, "Sleep structure in patients with psychogenic nonepileptic seizures," *Epilepsy Behav.*, vol. 4, no. 4, pp. 395–398, Aug. 2003.

[6] A. Staniszewska, A. Mąka, U. Religioni, and D. Olejniczak, "Sleep disturbances among patients with epilepsy," *Neuropsychiatr. Dis. Treat.*, vol. 13, pp. 1797–1803, July 2017.

[7] R. Khatami, D. Zutter, A. Siegel, J. Mathis, F. Donati, and C. L. Bassetti, "Sleep-wake habits and disorders in a series of 100 adult epilepsy patients--a prospective study," *Seizure*, vol. 15, no. 5, pp. 299–306, July 2006.

[8] M. Choy *et al.*, "Repeated hippocampal seizures lead to brain-wide reorganization of circuits and seizure propagation pathways," *Neuron*, vol. 110, no. 2, pp. 221-236.e4, Jan. 2022.

[9] A. Vezzani, J. French, T. Bartfai, and T. Z. Baram, "The role of inflammation in epilepsy," *Nat. Rev. Neurol.*, vol. 7, no. 1, pp. 31–40, Jan. 2011.

[10] X. Zhao *et al.*, "Noninflammatory changes of microglia are sufficient to cause epilepsy," *Cell Rep.*, vol. 22, no. 8, pp. 2080–2093, Feb. 2018.

[11] D. S. Reddy and R. Kuruba, “Experimental models of status epilepticus and neuronal injury for evaluation of therapeutic interventions,” *Int. J. Mol. Sci.*, vol. 14, no. 9, pp. 18284–18318, Sept. 2013.

[12] M. Vrinda, S. Arun, B. N. Srikumar, B. M. Kutty, and B. S. Shankaranarayana Rao, “Temporal lobe epilepsy-induced neurodegeneration and cognitive deficits: Implications for aging,” *J. Chem. Neuroanat.*, vol. 95, pp. 146–153, Jan. 2019.

[13] V. Sladky *et al.*, “Distributed brain co-processor for tracking spikes, seizures and behaviour during electrical brain stimulation,” *Brain Commun.*, vol. 4, no. 3, p. fcac115, May 2022.

[14] F. Mivalt *et al.*, “Electrical brain stimulation and continuous behavioral state tracking in ambulatory humans,” *J. Neural Eng.*, vol. 19, no. 1, p. 016019, Feb. 2022.

[15] V. Kremen *et al.*, “Integrating brain implants with local and distributed computing devices: A next generation epilepsy management system,” *IEEE J. Transl. Eng. Health Med.*, vol. 6, 2018.

[16] T. Denison and M. J. Morrell, “Neuromodulation in 2035: The neurology future forecasting series,” *Neurology*, vol. 98, no. 2, pp. 65–72, Jan. 2022.

[17] V. Sladky *et al.*, “Integrated human-machine interface for closed-loop stimulation using implanted and wearable devices,” presented at the 2022 IEEE International Conference on Systems, Man, and Cybernetics (SMC), 2022, pp. 1730–1735.

[18] M. J. Morrell and RNS Study Group, “Responsive cortical stimulation for the treatment of medically intractable partial epilepsy,” *Neurology*, vol. 77, no. 13, pp. 1295–1304, Sept. 2011.

[19] V. Salanova *et al.*, “The SANTÉ study at 10 years of follow-up: Effectiveness, safety, and sudden unexpected death in epilepsy,” *Epilepsia*, vol. 62, no. 6, pp. 1306–1317, June 2021.

[20] V. Salanova *et al.*, “Long-term efficacy and safety of thalamic stimulation for drug-resistant partial epilepsy,” *Neurology*, vol. 84, no. 10, pp. 1017–1025, Mar. 2015.

[21] R. Fisher *et al.*, “Electrical stimulation of the anterior nucleus of thalamus for treatment of refractory epilepsy: Deep Brain Stimulation of Anterior Thalamus for Epilepsy,” *Epilepsia*, vol. 51, no. 5, pp. 899–908, May 2010.

[22] D. R. Nair *et al.*, “Nine-year prospective efficacy and safety of brain-responsive neurostimulation for focal epilepsy,” *Neurology*, vol. 95, no. 9, pp. e1244–e1256, Sept. 2020.

[23] V. Kremen *et al.*, “Modulating limbic circuits in temporal lobe epilepsy: impacts on seizures, memory, mood and sleep,” *Brain Commun.*, vol. 7, no. 2, p. fcaf106, Apr. 2025.

[24] A. Pitkanen, P. A. Schwartzkroin, and S. L. Moshe, *Models of seizures and epilepsy*. London, England: Academic Press Inc. (London), 2006.

[25] W. Löscher and G. A. Worrell, “Novel subscalp and intracranial devices to wirelessly record and analyze continuous EEG in unsedated, behaving dogs in their natural environments: A new paradigm in canine epilepsy research,” *Front. Vet. Sci.*, vol. 9, p. 1014269, Oct. 2022.

[26] E. E. Patterson, “Canine epilepsy: an underutilized model,” *ILAR J.*, vol. 55, no. 1, pp. 182–186, 2014.

[27] J. J. Van Gompel *et al.*, “Swine model for translational research of invasive intracranial monitoring: Swine Animal Model for Translational Intracranial EEG,” *Epilepsia*, vol. 52, no. 6, pp. e49-53, June 2011.

[28] F. Zhu, H. Wang, L. Li, A. Bragin, D. Cao, and Y. Cheng, “Intracranial electrophysiological recordings on a swine model of mesial temporal lobe epilepsy,” *Front. Neurol.*, vol. 14, 2023.

[29] M. J. Silfverhuth *et al.*, “A characteristic time sequence of epileptic activity in EEG during dynamic penicillin-induced focal epilepsy--a preliminary study,” *Seizure*, vol. 20, no. 7, pp. 513–519, Sept. 2011.

[30] M. Lévesque and M. Avoli, “The kainic acid model of temporal lobe epilepsy,” *Neurosci. Biobehav. Rev.*, vol. 37, no. 10 Pt 2, pp. 2887–2899, Dec. 2013.

[31] I. Blümcke *et al.*, “A new clinico-pathological classification system for mesial temporal sclerosis,” *Acta Neuropathol.*, vol. 113, no. 3, pp. 235–244, Mar. 2007.

[32] H. Kitaura, H. Shirozu, H. Masuda, M. Fukuda, Y. Fujii, and A. Kakita, “Pathophysiological characteristics associated with epileptogenesis in human hippocampal sclerosis,” *EBioMedicine*, vol. 29, pp. 38–46, Mar. 2018.

[33] Y.-C. Wang *et al.*, “Probing circuit of Papez with stimulation of anterior nucleus of the thalamus and hippocampal evoked potentials,” *Epilepsy Res.*, vol. 159, no. 106248, p. 106248, Jan. 2020.

[34] K. Štillová *et al.*, “The role of anterior nuclei of the thalamus: A subcortical gate in memory processing: An intracerebral recording study,” *PLoS One*, vol. 10, no. 11, p. e0140778, Nov. 2015.

[35] A. V. Ulyanova *et al.*, “Electrophysiological signature reveals laminar structure of the porcine hippocampus,” *eNeuro*, vol. 5, no. 5, p. ENEURO.0102-18.2018, Sept. 2018.

[36] A. Bragin, J. Engel Jr, C. L. Wilson, E. Vizentin, and G. W. Mathern, “Electrophysiologic analysis of a chronic seizure model after unilateral hippocampal KA injection,” *Epilepsia*, vol. 40, no. 9, pp. 1210–21., 1999.

[37] L. Martinez-Ramirez, A. Slate, G. Price, A.-C. Duhaime, K. Staley, and B. A. Costine-Bartell, “Robust, long-term video EEG monitoring in a porcine model of post-traumatic epilepsy,” *eNeuro*, vol. 9, no. 4, p. ENEURO.0025-22.2022, June 2022.

[38] A. P. Jardim *et al.*, “Granule cell dispersion is associated with hippocampal neuronal cell loss, initial precipitating injury, and other clinical features in mesial temporal lobe epilepsy and hippocampal sclerosis,” *Seizure*, vol. 90, pp. 60–66, Aug. 2021.

[39] R. Janca *et al.*, *Automatic detection and spatial clustering of interictal discharges in invasive recordings*. 2013.

[40] A. H. Ayyoubi *et al.*, “Benchmarking signal quality and spatiotemporal distribution of interictal spikes in prolonged human iEEG recordings using CorTec wireless brain interchange,” *Sci. Rep.*, vol. 14, Feb. 2024.

[41] F. Mivalt *et al.*, “Impedance rhythms in human limbic system,” *J. Neurosci.*, vol. 43, no. 39, pp. 6653–6666, Sept. 2023.

[42] T. Denison, M. Koubeissi, E. Krook-Magnuson, D. Mogul, G. Worrell, and C. Schevon, “Stimulating Solutions for Intractable Epilepsy,” *Epilepsy Curr.*, vol. 21, no. 5, p. 15357597211012466, 2021.

[43] G. Ojeda Valencia *et al.*, “Signatures of electrical stimulation driven network interactions in the human limbic system,” *J. Neurosci.*, vol. 43, no. 39, pp. 6697–6711, Sept. 2023.

[44] F. Mivalt *et al.*, “Electrical brain stimulation and continuous behavioral state tracking in ambulatory humans,” *Journal of neural engineering*, vol. 19, no. 1, p. 016019, Feb. 2022.

[45] F. Mivalt *et al.*, “Automated sleep classification with chronic neural implants in freely behaving canines,” *J. Neural Eng.*, vol. 20, no. 4, Aug. 2023.

[46] I. Balzekas *et al.*, “Invasive Electrophysiology for Circuit Discovery and Study of Comorbid Psychiatric Disorders in Patients With Epilepsy: Challenges, Opportunities, and Novel Technologies,” *Front. Hum. Neurosci.*, vol. 15, p. 702605, 2021.

[47] U. Albus, “Guide for the Care and Use of Laboratory Animals (8th edn),” *Lab. Anim.*, vol. 46, no. 3, pp. 267–268, 2012.

[48] S. S. Grewal *et al.*, “Fast gray matter acquisition T1 inversion recovery MRI to delineate the mammillothalamic tract for preoperative direct targeting of the anterior nucleus of the thalamus for deep brain stimulation in epilepsy,” *Neurosurg. Focus*, vol. 45, no. 2, p. E6, Aug. 2018.

[49] A. Sudhyadhom, I. U. Haq, K. D. Foote, M. S. Okun, and F. J. Bova, “A high resolution and high contrast MRI for differentiation of subcortical structures for DBS targeting: the Fast Gray Matter Acquisition T1 Inversion Recovery (FGATIR),” *Neuroimage*, vol. 47 Suppl 2, pp. T44-52, Aug. 2009.

[50] J. K. Krauss *et al.*, “Technology of deep brain stimulation: current status and future directions,” *Nat. Rev. Neurol.*, vol. 17, no. 2, pp. 75–87, Feb. 2021.

[51] R. Kikinis, S. D. Pieper, and K. G. Vosburgh, “3D slicer: A platform for subject-specific image analysis, visualization, and clinical support,” in *Intraoperative Imaging and Image-Guided Therapy*, New York, NY: Springer New York, 2014, pp. 277–289.

[52] B. Felix, M. E. Leger, D. Albe-Fessard, J. C. Marcilloux, O. Rampin, and J. P. Laplace, “Stereotaxic atlas of the pig brain,” *Brain Res. Bull.*, vol. 49, no. 1–2, pp. 1–137, May 1999.

[53] H. M. Reimann and T. Niendorf, “The (Un)conscious mouse as a model for human brain functions: Key principles of anesthesia and their impact on translational neuroimaging,” *Front. Syst. Neurosci.*, vol. 14, p. 8, May 2020.

[54] J. Kang, H. Watanabe, and J. Shen, “Protocols for assessing neurodegenerative phenotypes in Alzheimer’s mouse models,” *STAR Protoc.*, vol. 2, no. 3, p. 100654, Sept. 2021.

[55] N. Pilati, M. Barker, S. Panteleimonitis, R. Donga, and M. Hamann, “A rapid method combining Golgi and Nissl staining to study neuronal morphology and cytoarchitecture,” *J. Histochem. Cytochem.*, vol. 56, no. 6, pp. 539–550, June 2008.

[56] Y. Liu *et al.*, “Development of the entorhinal cortex occurs via parallel lamination during neurogenesis,” *Front. Neuroanat.*, vol. 15, p. 663667, May 2021.

[57] C. R. Bjarkam, A. N. Glud, D. Orlowski, J. C. H. Sørensen, and N. Palomero-Gallagher, “The telencephalon of the Göttingen minipig, cytoarchitecture and cortical surface anatomy,” *Brain Struct. Funct.*, vol. 222, no. 5, pp. 2093–2114, July 2017.

[58] C. A. Schneider, W. S. Rasband, and K. W. Eliceiri, “NIH Image to ImageJ: 25 years of image analysis,” *Nat. Methods*, vol. 9, no. 7, pp. 671–675, July 2012.

Acknowledgement

This research was supported by NIH R01-NS092882, Birdel Fund Mayo Clinic Philanthropy and Cadence Neuroscience who provided the electrophysiology neural workstation and the INSR devices. We thank the XRI Core and Department of Comparative Medicine within Mayo Clinic for supporting our experiments. Figure drawings were made by the authors. The renderings of the workstation and implantable systems were provided by Cadence Neuroscience.

Data Availability

Data is available from the corresponding authors upon reasonable request.

Conflict of Interest

G.A.W., J.V.G have licensed intellectual property developed at Mayo Clinic to Cadence Neuroscience and to NeuroOne Inc. Mayo Clinic has received research support and consulting fees on behalf of G.A.W. from Cadence Neuroscience, NeuroOne, and Medtronic. F.M. received a salary support from Cadence Neuroscience Inc.

Author Contributions

FM, DM, SC, GW – creating figures, and writing the first draft of manuscript, incorporating suggestions and edits

GW, SC, NG, VKremen, KL – methodology, experimental design, supervision

IK, JVG, KM, JK - surgical protocol development & sterile surgery

FM, IK, JK, ADL, DMontonye, CG - animal care, data recording, charging of the implanted devices

FM, BW, VKrakorova – MRI data processing, image registration, rendering of Papez circuit using histology atlas (Figure 2)

CYK, FM – data annotation and validation of seizure and spike detectors

FM, PB, DM – electrophysiology data curation and analysis

GW, NG – electrophysiology data interpretation

DM, SC – histology protocol development and tissue (Figure 4)

ESH, SS, LHK – blinded analysis of histological slices

All authors participated in the manuscript editing.